Adaptive Self-Tuned Current Controller Design for an LCL-Filtered LC-Tuned Single-Phase Shunt Hybrid Active Power Filter

Mohammad-Sadegh Karbasforooshan, and Mohammad Monfared, *Senior Member, IEEE*

***Abstract*-- This paper proposes an adaptive self-tuned current controller design for an LCL-filtered LC-tuned single-phase shunt hybrid active power filter (HAPF), which offers adaptability and flexibility of the control system to filter parameters changes. System modelling and online identification of parameters are presented. Then, a systematic self-tuned controller (STC) design is proposed to calculate the controller parameters and obtain the final control law adaptively. The exact HAPF parameters design is described and the overall closed-loop stability evaluation with considering digital control delay is discussed in this paper. To confirm the theoretical achievements, simulations and experimental tests on a real prototype system are performed. The results are in good accordance and demonstrate the effectiveness and superior performance of the suggested control technique. Furthermore, a comprehensive comparison between the proposed control technique and other controllers is provided to show the superiority of the proposed system from different aspects.**

***Index Terms*-- Hybrid active power filter; adaptive controller; self-tuned controller; LCL filter; stability evaluation.**

NOMENCLATURE

PPF	Passive power filter
APF	Active power filter
HAPF	Hybrid active power filter
PI	Proportional-integral
PR	Proportional-resonant
STC	Self-tuned controller
FACTS	Flexible AC transmission system
ZOH	Zero-order hold
RLS	Recursive least square
MDDP	Minimum degree pole placement
ITAE	Integral time absolute error
PWM	Pulse-width modulation
PCC	Point of common coupling
THD	Total harmonic distortion
i_S	Source current
i_L	Load current
i_H	HAPF injected current
i_P	PPF inductor current
i_A	APF injected current
i_C	LCL filter capacitor current
i_I	Converter output current
v_S	Grid voltage
v_{conv}	Converter output voltage
v_{Cp}	PPF capacitor voltage
T_S	Sampling period

I. INTRODUCTION

PPFs, APFs and HAPFs are introduced to alleviate the effects of harmonic currents and reactive power issues of nonlinear loads in electrical networks. The PPFs have the advantages of simplicity, low cost, and high reliability; however, their performance highly depends on the grid and load conditions and they are susceptible to resonance with the grid [1]-[3]. The APFs have advantages of flexibility, perfect harmonic compensation and eliminating the possibility of any resonances. However, they suffer from lower reliability due to their active elements (power semiconductors), higher cost and lower rating due to semiconductors limitations [4]-[6]. The traditional HAPFs, which are a series connection of the PPF and the APF and are connected in parallel to the grid, are proposed for medium voltage and high power applications. In these structures, the fundamental component of the grid voltage drops across the PPF capacitor, hence the APF voltage significantly decreases. Still a high compensation current flows through the power switches, due to the series connection of the APF [7]-[16]. An improved HAPF structure, including the parallel connection of the APF with the PPF inductor, is presented in [17]-[19]. This structure offers a lower APF current rating and higher reliability than the conventional HAPFs. While a complex reference current generation and control system are proposed for the improved HAPF, the parameter uncertainties and the effect of grid impedance variations are not investigated yet. The complex parameter and control design and probably the higher implementation cost can be mentioned as major limitations of the improved HAPFs. The single-phase shunt HAPF can be used for compensating nonlinear loads of domestic or commercial consumers. Although the THD of each low-power single-phase nonlinear load (such as computers, CFLs, LEDs, refrigerators, TVs, air conditioners and so on) is high, the RMS values are low. When all these loads are supplied

Mohammad-Sadegh Karbasforooshan and Mohammad Monfared are with the Department of Electrical Engineering, Faculty of Engineering, Ferdowsi University of Mashhad, Mashhad, Iran (e-mail: s.karbasforooshan@mail.um.ac.ir; m.monfared@um.ac.ir).

at the same time in a domestic or commercial complex, then the values of both THD and RMS current are high. The single-phase HAPFs can be used in three-phase four-wire distribution networks.

To control the HAPF system, many different techniques such as proportional (P) [7]-[9], PR [5], [10], [19], repetitive [11], deadbeat [6], [12], fuzzy [13], predictive [14], and nonlinear controllers [15]-[16] are employed to track the reference current and reject disturbances. Resonant controllers provide a high gain at the desired frequency and its multiples [5]. This type of controller has the advantages of simplicity, relatively fast dynamic response and low computational burden, but they suffer from decaying response reduction to step changes, high sensitivity to the grid frequency changes and instability due to the phase shift [5], [10], [19]. Repetitive controllers are a common type of controllers in reference tracking of periodic signals. Their transfer functions are basically equal to the sum of a high number of harmonic resonators. Repetitive controllers benefit from high tracking accuracy and simple implementation, but their limitations are slow dynamic response and high memory space occupation [11]. The deadbeat controller is a digital model-based controller which offers high control precision and fast dynamic response; while its performance is highly dependent on the model parameters [6]. Adaptive control methods are widely used in industry and academia and STC is a well-established adaptive method, which has shown success in many applications [20]-[26]. In [20] and [21], the authors use STC to control a DC-DC switching converter. The average model of the non-inverting buck-boost converter in the time domain is obtained in [20]. Then, RLS system identification and the STC method are implemented. However, calculations of the final STC parameters for the digital system, and the control stability evaluation are missing. Also, the mathematical and identified model parameters are relatively different. Authors in [21] estimate the synchronous buck DC-DC converter parameters using Kalman filter and then implement the STC technique to obtain the final duty cycle of the converter switch. In this paper, much efforts have been made in Kalman filter improvement for the parameters estimation and a brief on STC and control system is presented. Reference [22] discusses high-precision position control of a switched reluctance motor using the STC method. In this paper, only the fundamental formula for the parameter estimation and the STC are reported without any model and controller calculations. References [23]-[26] discuss using STC for FACTS devices (SVC, TCSC, STATCOM and UPFC). The exact system modelling in the discrete-time domain, the overall system stability evaluation, the effect of the system parameters changes on control performance and a comprehensive comparison between the proposed method and other control methods are not still addressed.

In the HAPF system like other mentioned systems, the exact values of the inductors and capacitors may not be always known. In practice, they are affected by several factors, such as manufacturing tolerances, ageing, temperature, deterioration and load level. With the model-based controllers, any difference between the nominal values, which are considered in the controller design, and the actual values affects the compensation performance and may even lead to instability. Also, in other non-model-based techniques, the effect of system parameters changes on control performance can be relatively significant. Indeed, the control parameters are designed for the current situation and continuous modification should be applied over time.

This paper proposes an adaptive STC control technique for the single-phase LCL-filtered HAPF. In the proposed technique, the reference current tracking of the HAPF and the grid current compensation are adaptively performed such that possible changes or mismatches in the filter parameters do not degrade the control system performance. Also, the digital nature of the proposed controller simplifies its implementation.

In this paper, the system is modelled in the continues-domain and then transformed into a discrete-time form. Then, a straightforward online identification algorithm for the system parameters is proposed followed by a systematic design procedure for an adaptive STC for the APF injected current. Therefore, the effect of system parameters' mismatches is compensated for. Also, improved formula for the adaptive control law is suggested, which ensures proper rejection of grid voltage disturbances. Then, the HAPF parameters design is described considering the LCL filter stability requirements. Afterwards, the overall closed-loop control stability in the discrete domain and considering the digital control delay is discussed. Finally, simulation and experimental results on a real prototype under steady-state and transient circumstances, including model parameters' changes are reported. That confirm the superior performance of the developed control scheme. Also, a comparison between the suggested technique and other control methods is provided. The original contributions of this work can be summarized as:

- exact modelling of the LCL-filtered LC-tuned single-phase shunt HAPF;
- online identification of system parameters;
- proposing a systematic and straightforward procedure for STC design;
- proposing an improved formula for the adaptive control law to reject grid voltage disturbances;
- designing a stable LCL filter without any extra passive or active damping methods;
- evaluating the effectiveness and superiority of the proposed technique over other successful current controllers under various conditions.

II. System Modelling and Identification

The single-tuned single-phase shunt improved HAPF structure is shown in Fig. 1. In this structure, a single-tuned PPF is connected to the grid and a single-phase APF is in parallel with the PPF inductor. Besides, an LCL-type switching noise smoothing filter is employed at the converter output. The LCL filter capacitor is very small and shows its effect at high frequencies. So, due to its high impedance at low frequencies and a negligible current through it, its effect is neglected in the following modelling and controller design. Although, the exact modelling, HAPF parameters design and stability evaluation in

This article has been accepted for publication in a future issue of this journal, but has not been fully edited. Content may change prior to final publication. Citation information: DOI 10.1109/TPWRD.2021.3115661, IEEE Transactions on Power Delivery

presence of the LCL filter capacitor are performed in the next sections. Therefore, L_T accounts for both converter-side and grid-side inductors and equals to (L_A + L_I). The state-space continues-time model of the single-phase shunt HAPF is obtained as

$$\begin{cases} \dfrac{dx(t)}{dt} = \underbrace{\begin{bmatrix} 0 & 0 & \dfrac{1}{L_T} \\ 0 & 0 & \dfrac{1}{L_P} \\ \dfrac{-1}{C_P} & \dfrac{-1}{C_P} & 0 \end{bmatrix}}_{A} x(t) + \underbrace{\begin{bmatrix} \dfrac{1}{L_T} \\ 0 \\ 0 \end{bmatrix}}_{B} v_{conv}(t) + \underbrace{\begin{bmatrix} \dfrac{-1}{L_T} \\ \dfrac{-1}{L_P} \\ 0 \end{bmatrix}}_{B_v} v_S(t) \\ y(t) = \underbrace{\begin{bmatrix} 1 & 0 & 0 \end{bmatrix}}_{C_o} x(t) \end{cases} \quad (1)$$

where $x(t)=[i_A(t)\ i_P(t)\ v_{CP}(t)]^T$ is the state vector. By applying the Laplace operator to (1), the transfer functions of the converter and grid voltages to the APF current can be calculated as

$$i_A(s) = \underbrace{\frac{L_P C_P s^2 + 1}{L_T L_P C_P s^3 + (L_T + L_P)s}}_{G_{plant}(s)} v_{conv}(s) \quad (2)$$

$$i_A(s) = -\frac{L_P C_P s^2}{L_T L_P C_P s^3 + (L_T + L_P)s} v_S(s). \quad (3)$$

The ZOH method is the most common discretization technique, which is widely utilized in industrial control systems to discretize the plant model wherever a digital platform is employed to implement the digital control algorithm. By discretizing the continues-time model of (2) using the ZOH method, the discrete-time model of the HAPF system yields as

$$G_{plant}(z) = \frac{i_A(z)}{v_{conv}(z)} = \frac{B(z)}{A(z)} = \frac{b_1 z^2 + b_2 z + b_1}{z^3 - a_1 z^2 + a_1 z - 1}$$

$$\begin{cases} b_1 = \dfrac{\alpha L_T T_S + L_P \sin(\alpha T_S)}{\alpha L_T (L_T + L_P)}, \ a_1 = 2\cos(\alpha T_S) + 1 \\ b_2 = -2\dfrac{\alpha L_T T_S \cos(\alpha T_S) + L_P \sin(\alpha T_S)}{\alpha L_T (L_T + L_P)}, \ \alpha = \sqrt{\dfrac{L_T + L_P}{L_T L_P C_P}} \end{cases}. \quad (4)$$

As can be seen in (4), there are three independent parameters in the discrete-time transfer function. To have an accurate estimation of these parameters and design the controller, the system should be identified online. The identified parameters depend on the values of the PPF inductor and capacitor, the APF output inductor and T_S. Any changes in these three system elements and the sampling period must directly reflect in the discrete-time model. Then, the designed controller can stabilize the system and track the reference waveform perfectly. The difference equation of (4) is

$$\underbrace{\left(i_A(k) - i_A(k-3)\right)}_{\tilde{i}_A(k)} = a_1\left(i_A(k-1) - i_A(k-2)\right) + b_1\left(v_{conv}(k-1) + v_{conv}(k-3)\right) + b_2 v_{conv}(k-2). \quad (5)$$

Therefore, the identification regression vector can be written as

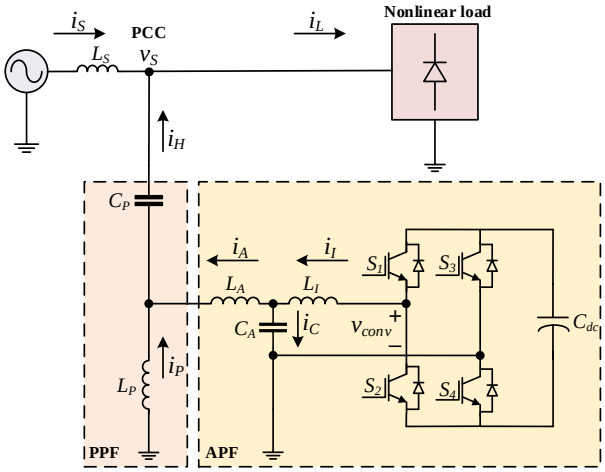

Fig. 1. Single-tuned single-phase shunt improved HAPF structure.

$$\varphi(k) = \begin{bmatrix} \left(i_A(k-1) - i_A(k-2)\right) \\ \left(v_{conv}(k-1) + v_{conv}(k-3)\right) \\ v_{conv}(k-2) \end{bmatrix} \quad (6)$$

and the identification parameters are

$$\theta^T(k) = \begin{bmatrix} a_1 & b_1 & b_2 \end{bmatrix}. \quad (7)$$

The RLS estimation algorithm for the system identification is then written as

$$\begin{cases} \hat{\theta}(k) = \hat{\theta}(k-1) + K(k)\left(\tilde{i}_A(k) - \varphi^T(k)\hat{\theta}(k-1)\right) \\ K(k) = P(k-1)\varphi(k)\left(\lambda I + \varphi^T(k)P(k-1)\varphi(k)\right)^{-1} \\ P(k) = \left(I - K(k)\varphi^T(k)\right)P(k-1)/\lambda \end{cases} \quad (8)$$

where λ is the forgetting factor of the algorithm. This algorithm ensures that the values of system parameters are continually updated while the recent data have more weight than the old data [27]. So, one can write

$$\begin{bmatrix} \hat{a}_1(k) \\ \hat{b}_1(k) \\ \hat{b}_2(k) \end{bmatrix} = \begin{bmatrix} \hat{a}_1(k-1) \\ \hat{b}_1(k-1) \\ \hat{b}_2(k-1) \end{bmatrix} + K(k) \begin{pmatrix} \tilde{i}_A(k) - \hat{a}_1(k-1) \times (i_A(k-1) \\ -i_A(k-2)) - \hat{b}_1(k-1) \times \\ (v_{conv}(k-1) + v_{conv}(k-3)) \\ -\hat{b}_2(k-1) \times v_{conv}(k-2) \end{pmatrix}$$

$$K(k) = \frac{P(k-1)\varphi(k)}{\lambda + \varphi^T(k)P(k-1)\varphi(k)}. \quad (9)$$

$$P(k) = \left(I_3 - K(k) \begin{bmatrix} i_A(k-1) - i_A(k-2) \\ v_{conv}(k-1) + v_{conv}(k-3) \\ v_{conv}(k-2) \end{bmatrix}^T \right) \frac{P(k-1)}{\lambda}$$

The system online identification algorithm is depicted in Fig. 2.

III. Indirect STC Design

Figure 3 shows the system structure with the proposed indirect STC. In this technique, the system parameters are first estimated online, as detailed before. Then, the *S*, *T* and *C* parameters of the controller are designed and finally, the control

This article has been accepted for publication in a future issue of this journal, but has not been fully edited. Content may change prior to final publication. Citation information: DOI 10.1109/TPWRD.2021.3115661, IEEE Transactions on Power Delivery

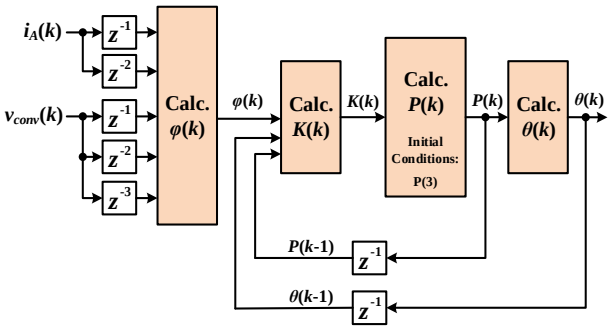

Fig. 2. System online identification algorithm.

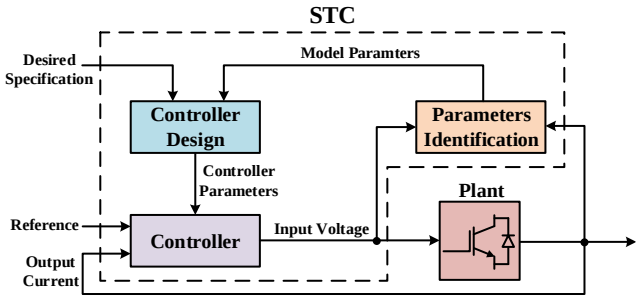

Fig. 3. System structure with proposed indirect STC.

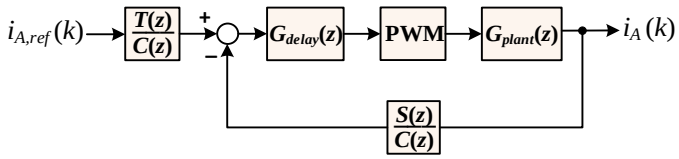

Fig. 4. Closed-loop current control diagram.

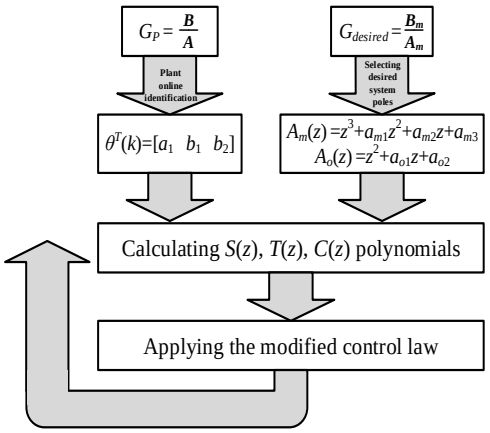

Fig. 5. Overall design steps flowchart.

system law is applied. The closed-loop controller diagram is shown in Fig. 4. The STC design characteristics are the desired closed-loop model which is obtained by MDDP and desired observer polynomial [27]. A systematic design procedure of the STC parameters is presented in this section. According to Fig. 3 and the STC theory, one can write

$$i_A(k) = \frac{BT}{AC + BS} i_{A,ref}(k). \tag{10}$$

where B and A are numerator and denominator of the plant model, respectively. The denominator of (10), i.e. (D_c=AC+BS) implies that the desired closed-loop characteristics are determined by C and S polynomials. The nominator of (10) has an important role in reference tracking. Also, the dynamics of the desired system response to the reference changes is

$$i_A(k) = \frac{B_m}{A_o A_m} i_{A,ref}(k) \tag{11}$$

where B_m, A_m, A_o are numerator, denominator, and observer of the desired discrete-time model, respectively. Equations (10) and (11) show that the command signal of the closed-loop system will be tracked if BT=B_m. The B polynomial relates to the plant, while T polynomial is a design parameter and should be determined to ensure accurate tracking of the reference signal. The denominator of (10) specifies the closed-loop poles of the system. The denominator of the desired discrete-time model is assumed as

$$A_m(z) = z^3 + a_{m1}z^2 + a_{m2}z + a_{m3} \tag{12}$$

where a_{m1}=-(z_1 + z_2 + z_3), a_{m2}=(z_1z_2 + z_1z_3 + z_2z_3), a_{m3}=-$z_1z_2z_3$ and z_1, z_2 and z_3 are the desired places of the system poles. The ITAE can be used to specify the dynamic response of the suggested system with relatively small overshoot and little oscillations. The optimum coefficients of the third-order system according to the ITAE criterion are [28]

$$D(s) = s^3 + 1.75\omega_n s^2 + 2.15\omega_n^2 s + \omega_n^3 \tag{13}$$

where ω_n is the natural frequency and is inversely proportional to the rise time of the system step response and must be chosen enough below the switching (sampling) frequency to prevent the switching noises from penetrating the controller. A tradeoff between fast dynamic performance and switching noise immunity can be achieved by setting ω_n equal to 10% of the sampling frequency (f_S). Then, the three poles in the s-domain are transformed into the z-domain by the transformation z=e^{sTs}.

The nominator polynomial of the desired discrete-time model is calculated as

$$\begin{cases} B^+(z) = 1 \\ B^-(z) = b_1 z^2 + b_2 z + b_1 \\ B'_m(z) = \dfrac{A_m(1)}{B^-(1)} z^{\deg(B^+)} = \dfrac{1 + a_{m1} + a_{m2} + a_{m3}}{2b_1 + b_2} \\ B_m(z) = B^- B'_m = \dfrac{1 + a_{m1} + a_{m2} + a_{m3}}{2b_1 + b_2}\left(b_1 z^2 + b_2 z + b_1\right) \end{cases}. \tag{14}$$

The degree of the desired closed-loop polynomial is obtained as 5. So, the degree of the desired observer polynomial is 2 and its polynomial is

$$A_o(z) = z^2 + a_{o1}z + a_{o2} \tag{15}$$

According to [27], the C, S and T polynomials are

$$C(z) = z^2 + c_1 z + c_2 \tag{16}$$

$$S(z) = s_0 z^2 + s_1 z + s_2 \tag{17}$$

$$T(z) = B'_m(z)A_o(z) = \frac{1 + a_{m1} + a_{m2} + a_{m3}}{2b_1 + b_2}\left(z^2 + a_{o1}z + a_{o2}\right). \tag{18}$$

To calculate the STC parameters, the Diophantine equation should be solved as

$$AC + BS = A_o A_m \tag{19}$$

that results in

This article has been accepted for publication in a future issue of this journal, but has not been fully edited. Content may change prior to final publication. Citation information: DOI 10.1109/TPWRD.2021.3115661, IEEE Transactions on Power Delivery

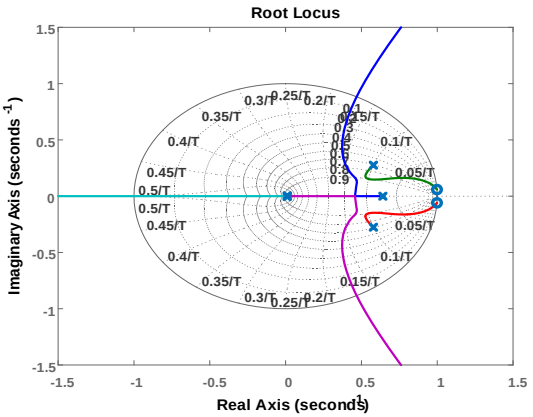

Fig. 6. Root locus of the desired closed-loop system.

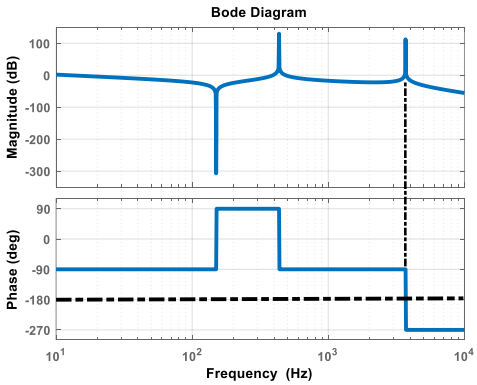

Fig. 7. Bode diagram of (28).

$$\begin{bmatrix} c_1 \\ c_2 \\ s_0 \\ s_1 \\ s_2 \end{bmatrix} = \begin{bmatrix} 1 & 0 & b_1 & 0 & 0 \\ -a_1 & 1 & b_2 & b_1 & 0 \\ a_1 & -a_1 & b_1 & b_2 & b_1 \\ -1 & a_1 & 0 & b_1 & b_2 \\ 0 & -1 & 0 & 0 & b_1 \end{bmatrix}^{-1} \begin{bmatrix} a_1 + a_{m1} + a_{o1} \\ \left(-a_1 + a_{m2} + a_{o1}a_{m1}\right) \\ +a_{o2} \\ \left(1 + a_{m3} + a_{o1}a_{m2}\right) \\ +a_{o2}a_{m1} \\ a_{o1}a_{m3} + a_{o2}a_{m2} \\ a_{o2}a_{m3} \end{bmatrix} . \quad (20)$$

Therefore, first, the AB polynomials of the discretized plant are identified by the RLS technique (equation (4)). Then, the STC parameters are determined from (20). Finally, the following law will be applied to obtain the PWM control signal [27]:

$$Cu(k) = Ti_{A,ref}(k) - Si_A(k) \quad (21)$$

Therefore

$$u(k) = -c_1u(k-1) - c_2u(k-2) + t_0i_{A,ref}(k) + t_1i_{A,ref}(k-1) + t_2i_{A,ref}(k-2) - s_0i_A(k) - s_1i_A(k-1) - s_2i_A(k-2) \quad (22)$$

where

$$t_0 = \frac{t_1}{a_{o1}} = \frac{t_2}{a_{o2}} = \frac{1 + a_{m1} + a_{m2} + a_{m3}}{2b_1 + b_2} . \quad (23)$$

To reject the grid voltage disturbances, the grid voltage at the PCC is measured and the control input is corrected accordingly as

$$\begin{cases} x(k+1) = A_d x(k) + B_d u(k) + B_{dv} v_S(k) \\ u(k) = u'(k) - B_d^{-1} B_{dv} v_S(k) \end{cases} \quad (24)$$

where $u'(k)$ is the left-hand side of (22). Figure 5 shows the overall design steps flowchart. Figure 6 shows the root locus of the desired closed-loop system of (11). As can be observed, all the closed-loop poles are inside the unit circle with the desired damping, translating to a stable system.

IV. Design Considerations

A. LC-Tuned Filter Design

The design of the single-tuned PPF parameters must be done according to the nonlinear load characteristics and compensation requirements, especially the dominant load harmonic order and the required reactive power compensation. The capacitor C_P is chosen according to the required reactive power and the series connection of C_P and L_P is then tuned for selective compensation of the major load harmonic of concern.

B. LCL Filter Design

To design the LCL output filter of the converter, many constraints such as reactive power produced by the filter capacitor, converter current ripple, switching harmonics injected to the grid, total inductance of the filter, the value of resonance frequency are considered in the literature [29]-[31]. According to a procedure developed in [32], the reactive power of the capacitor is limited to a percentage of the nominal converter power, x_1. Also, the converter current ripple is limited to a percentage of the nominal peak current, x_2 and the harmonic currents injected to the grid, which their order is greater than 35 must be limited to a percentage of the nominal current according to IEEE 519 standard, here denoted by x_3. These constraints are described for the suggested HAPF in (25)-(27) where usually x_1=0.025-0.05, x_2=0.15-0.4, x_3=0.003 and V_{LP}, S_{rated}, $I_{P,rated}$ and $V_{sb1,\max}$ are the RMS voltage across the PPF inductor, converter nominal power, converter nominal peak current and the maximum value of harmonic components at the first switching sideband, respectively.

$$\left(2\pi f_1 C_A V_{L_P}^2\right) \le x_1 S_{rated} \quad (25)$$

$$\left(\Delta i_{I,\max} = \frac{V_{dc}T_S}{8L_I}\right) \le x_2 I_{P,rated} \quad (26)$$

$$\left(i_{A,sb1,\max} = G_{i_A - v_{conv},HF} V_{sb1,\max}\right) \le x_3 I_{P,rated} . \quad (27)$$

It has been confirmed that the system will be stable in presence of digital delay if the resonance frequency lies in the range $f_S/6<f_{res}<f_S/2$ [32]-[34]. Considering the effects of the LCL filter capacitor (C_A) and the grid impedance (L_S) in (1), the transfer function of the converter voltage to the APF current can be calculated as

$$G_{plant}(s) = \frac{i_A(s)}{v_{conv}(s)} = \frac{(L_P + L_S)C_P s^2 + 1}{D_1(s)}$$
$$D_1(s) = \left(L_I(L_AL_P + L_AL_S + L_PL_S)C_AC_P\right)s^5 + \left((L_A + L_P)L_IC_A + (L_I + L_A)L_PC_P + (L_I + L_A + L_P)L_SC_P\right)s^3 + (L_I + L_A + L_P)s \quad . (28)$$

Figure 7 shows the Bode diagram of (28). This figure shows one trap whose frequency is related to the PPF parameters and

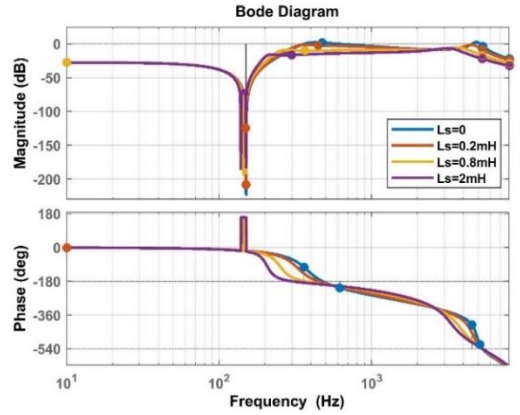

Fig. 8. Bode diagram of the open-loop current control system for different values of L_S (grid impedance).

TABLE I
System Parameters

Parameter	Symbol	Value
Grid voltage (RMS)	V_S	230 Vrms
Grid frequency	f	50 Hz
Converter nominal power	S_{rated}	0.5 kVA
DC-link voltage	V_{dc}	150 V
PPF capacitor	C_P	100 μF
PPF inductor	L_P	11.2 mH
LCL grid-side inductor	L_A	0.75 mH
LCL inverter-side inductor	L_I	0.75 mH
LCL capacitor	C_A	5 μF
Switching/sampling frequency	f_{sw}/f_s	8/16 kHz
Nonlinear load DC-side RC	R/C	10 Ω/2200 μF

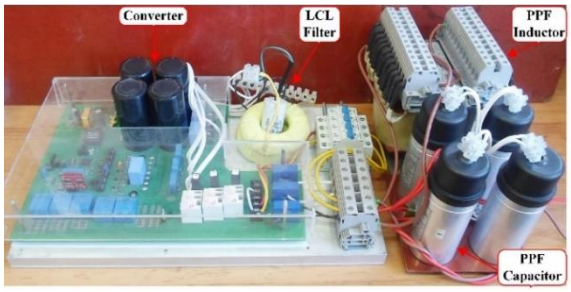

Fig. 9. Experimental setup.

two other resonance peaks, which are due to the LCL filter. In this condition, $G_{plant}(s)$ is unstable; because the magnitude characteristic is greater than zero when the phase diagram crosses -180º at the second resonance frequency. Also, the first resonance frequency does not affect the stability of $G_{plant}(s)$.

The possible range of change of resonance frequencies due to the grid impedance can be obtained by subtitling L_S=0 and L_S=∞ into conjugate poles of $D_I(s)$. Because the first resonance frequency does not affect the stability of the system, the following two constraints for the second resonance frequency are calculated.

$$\frac{L_I+L_A+L_P}{L_I(L_A+L_P)C_A} \ge \left(2\pi\frac{f_s}{6}\right)^2 \tag{29}$$

$$\left(\frac{1}{2L_IC_A}+\frac{L_AC_A+L_PC_A+L_PC_P}{2L_AL_PC_AC_P} + \frac{\sqrt{\left(-(L_A+L_P)L_IC_A+(L_A+L_I)L_PC_P\right)^2+4L_I^2L_P^2C_AC_P}}{2L_IL_AL_PC_AC_P}\right) \le \left(2\pi\frac{f_s}{2}\right)^2. \tag{30}$$

So, the final value of LCL parameters can be designed in the following way: first, the capacitor value should meet both following practical and stability constraints:

$$\begin{cases} C_A \le \dfrac{x_1 S_{rated}}{\omega_1 V_{L_P}^2} \\ C_A \le \dfrac{V_{dc}T_S + 8x_2 I_{P,rated}(L_A+L_P)}{V_{dc}T_S(L_A+L_P)\omega_{\min}^2} \end{cases} \tag{31}$$

where $\omega_{\min}$ equals $2\pi(f_S/6)$. The second constraint is obtained by substituting L_I from (26) into (29). Then, the value of the converter-side inductor is calculated as

$$L_I = \frac{1}{C_A\omega_{\min}^2}. \tag{32}$$

It should be noticed that the allowable current ripple for L_I is considered in the calculation of C_A. Finally, the grid-side inductor should meet the below constraint

$$L_A \ge \frac{V_{sb1,\max}}{L_IC_A\omega_s^3 x_3 I_{P,rated}}. \tag{33}$$

C. APF Reference Current Generation

To generate the reference current of the APF, first, the load harmonic components must be extracted. The load current harmonics are extracted by using the successful multi-second order generalized integrator (MSOGI) technique. This is a well-documented technique that has already been proved to be a superior solution for precise extraction of the harmonic components of a voltage or current waveform [6], [35]-[36]. In this technique, the in-phase (α-axis) harmonic components to be compensated by the HAPF are extracted individually and the sum of these components forms the reference current of the HAPF. With the APF in the circuit, the APF reference current is calculated by subtracting the measured PPF inductor current from the HAPF reference current.

D. Stability Evaluation

The diagram of the proposed current control is depicted in Fig. 4, where $G_{delay}(z) = z^{-T_d/T_S}$ represents the digital control delay (T_d is the total control system delay and is assumed as $1.5T_S$ for a double-updated PWM modulator), PWM modulator is considered as a unity gain and $G_{plant}(z)$ is the plant discretized model. According to Fig. 4, the closed-loop current control transfer function is calculated as

$$H_{closed}(z) = \frac{i_A(k)}{i_{A,ref}(k+1)} = \frac{T(z)G_{delay}(z)G_{plant}(z)}{C(z)+S(z)G_{delay}(z)G_{plant}(z)} \tag{34}$$

If the digital delay is ignored and $G_{plant}(z)$ is simply

This article has been accepted for publication in a future issue of this journal, but has not been fully edited. Content may change prior to final publication. Citation information: DOI 10.1109/TPWRD.2021.3115661, IEEE Transactions on Power Delivery

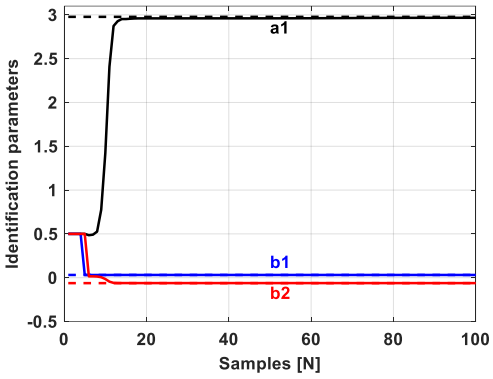

Fig. 10. HAPF identified parameters.

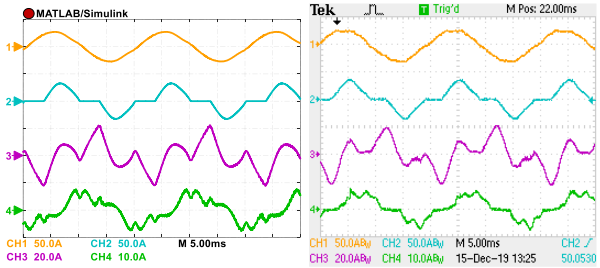

(a) (b)

Fig. 11. Steady-state performance of single-phase HAPF (a) simulation (b) experiment: grid current (50A/div) (17.6A_{rms}), load current (50A/div) (17.2A_{rms}), PPF inductor current (20A/div) (9.2A_{rms}) and APF injected current (10A/div) (3.1A_{rms}).

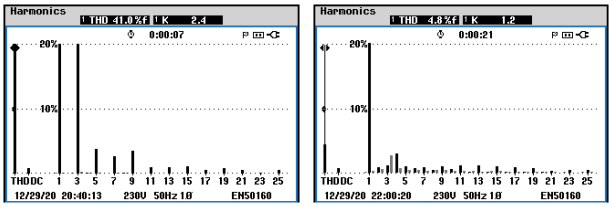

(a) (b)

Fig. 12. Steady-state experimental harmonic spectrums of the grid current: (a) before, and (b) after HAPF compensation.

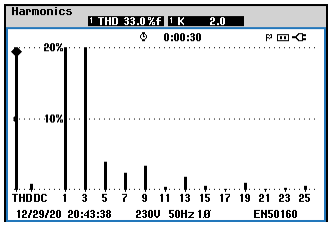

Fig. 13. Steady-state experimental harmonic spectrums of the grid current when only PPF is connected to grid.

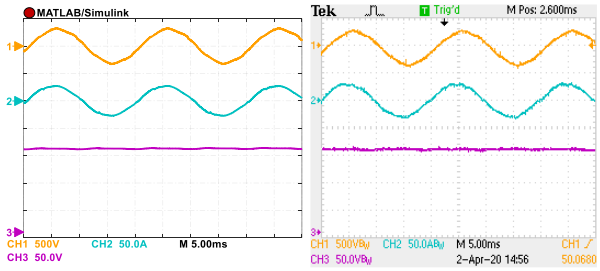

(a) (b)

Fig. 14. Steady-state performance of single-phase HAPF (a) simulation (b) experiment: grid voltage (500V/div) (230V_{rms}), grid current (50A/div) (17.6A_{rms}), and DC-link voltage (50V/div) (150V).

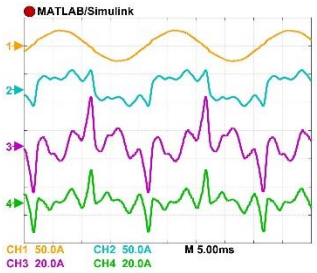

Fig. 15. Steady-state simulated performance of single-phase HAPF: grid current (50A/div) (19.1A_{rms}), load current (50A/div) (20.8A_{rms}), PPF inductor current (20A/div) (7.3A_{rms}) and APF injected current (20A/div) (6.6A_{rms}).

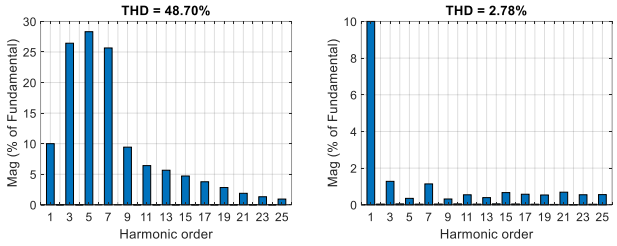

(a) (b)

Fig. 16. Steady-state simulation harmonic spectrums of the grid current: (a) before, and (b) after HAPF compensation.

considered as (4), equation (34) will be equal to (10)/(11) and the control system will be stable with desired characteristics. Figure 8 shows the open-loop Bode diagram of the HAPF current control system (34) for different values of grid impedance. When L_S increases from 0 to 2mH, the resonance frequencies slightly decrease. In these conditions, the overall control system with considering digital delay is stable without any extra passive or active damping techniques. An inherent delay-based damping method in this paper ensures that the phase lies between -180º and -540º at the second resonance frequency (where the amplitude may be greater than zero). In addition, the proposed current control system damps the first and the second resonances, appropriately.

V. Performance Evaluation

Simulations are done in MATLAB/Simulink environment. The system parameters are listed in Table I. A laboratory setup is also built, which is shown in Fig. 9. The nonlinear load consists of a single-phase diode rectifier feeding a resistor in parallel with a capacitor. The presence of the grid impedance results in the grid voltage distortions at the PCC. The HAPF identified parameters are shown in Fig. 10. As can be observed, the filter parameters are estimated quickly and accurately. The steady-state simulated and experimental performance of the single-phase shunt HAPF is shown in Fig. 11 that are in good accordance and demonstrate the effectiveness of the proposed control technique. The HAPF operation causes the grid current to become a high-quality sinusoidal waveform with THD = 4.8% (in the experiments), while the load current THD is 41%. Figures 12(a) and (b) show the harmonic spectrums of the grid current, before and after HPAF compensation, respectively. If the PPF is only connected to the grid, the grid current THD is 33% and the grid harmonic spectrum is shown in Fig. 13. As can be seen in this figure, the single-tuned PPF could not eliminate the 3rd harmonic component as it was expected under

This article has been accepted for publication in a future issue of this journal, but has not been fully edited. Content may change prior to final publication. Citation information: DOI 10.1109/TPWRD.2021.3115661, IEEE Transactions on Power Delivery

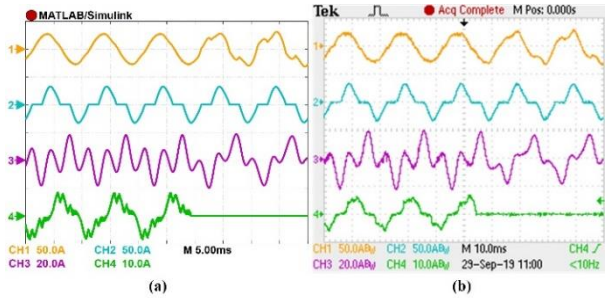

Fig. 17. Transient performance of single-phase HAPF in response to APF disconnection (a) simulation (b) experiment: grid current (50A/div), load current (50A/div), PPF inductor current (20A/div) and APF injected current (10A/div).

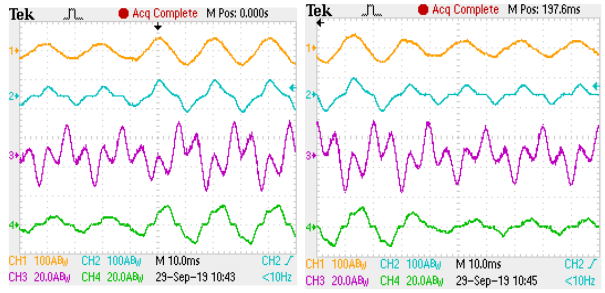

Fig. 18. Transient performance of single-phase HAPF in response to load step change in experiment (a) load increase (b) load decrease: grid current (100A/div), load current (100A/div), PPF inductor current (20A/div) and APF injected current (20A/div).

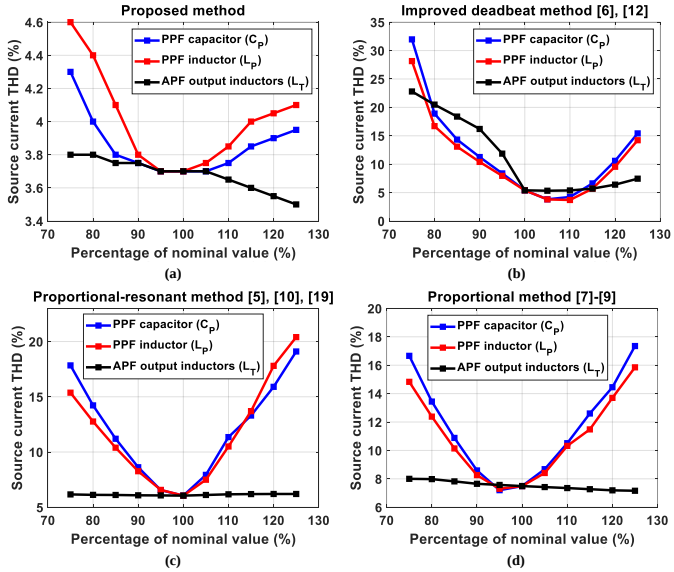

Fig. 19. Effect of HAPF parameters changes on source current THD: (a) proposed method, (b) improved deadbeat method [6], [12], (c) PR method [5], [10], [19], and (d) proportional method [7]-[9].

an ideal grid condition and the grid current THD is just slightly decreased from 41% to 33%. The grid voltage, current and DC-link voltage waveforms are shown together in Fig. 14. The peak-to-peak ripple of the DC-link voltage is below 2%. It should be emphasized that the DC-link voltage of the APF is readily kept fixed at the desired level by using a PI controller. The output signal of the PI controller is multiplied by the fundamental component of the grid voltage and is added to the APF reference current. Furthermore, the proposed scheme is compared to a single-phase traditional APF from different aspects. The DC-link voltage of the APF is practically selected in the range of 380V-400V. However, with the proposed HAPF structure, the fundamental component of the grid voltage drops across the PPF capacitor and the APF DC voltage requirement decreases significantly. Accordingly, it is set at 150V in this work. Also, due to the parallel connection of the PPF inductor and the APF, the APF current is significantly decreased. The RMS injected current of the APF in this study is 3.10A, but for a single-phase conventional APF it is 6.5A (for the same nonlinear load and the same expected compensation result). Thus, the converter power of the proposed HAPF is 310VA, while for the single-phase simple APF is 1800VA (almost 5-times higher). Also, if a problem or a semiconductor switch failure occurs, the whole harmonic compensation of the single-phase APF is lost, while the PPF part of the proposed HAPF still works with the level of compensation provided by the tuned components. Also, the proposed structure offers a lower converter current rating than the conventional HAPFs (HAPFs with a series connection of the PPF and the APF). Therefore, the power semiconductors' voltage and current ratings, the filter inductors' currents, the core size, the output filter and DC-link capacitors' voltage and sensors' ratings, heatsink dimensions, the power circuit PCB size, etc are considerably reduced. So, the overall cost of the proposed system is lower.

The steady-state simulated performance of the proposed shunt HAPF for a nonlinear load that contains a higher level of harmonics other than the 3rd component is shown in Fig. 15. Also, Figs. 16(a) and (b) show the harmonic spectrums of the grid current in this situation, before and after HPAF compensation, respectively. As evident, the proposed HAPF can effectively compensate for all harmonics and the grid current THD is reduced from 48.7% to 2.78%.

The transient behaviour of the system in response to the APF disconnection is studied and the results are shown in Figs. 17 (a) and (b). As can be seen, the quality of the source current is not acceptable when only the PPF operates and its THD is around 33%. The transient performance of the system in response to the load step changes in experiments is also shown in Figs. 18 (a) and (b). In these figures, the load current increases and decreases suddenly (with a circuit breaker). As can be seen, the APF injected current changes fast and smoothly and the grid current quality is not adversely affected. These waveforms imply that the APF harmonic mitigation speed is fast such that the tracking error settles in less than half a fundamental cycle.

Finally, to analyze the performance of the proposed controller in the presence of model parameters uncertainties, the effect of the parameters changes on the source current THD is studied and the results for the proposed method and three different successful current controllers are depicted in Fig. 19. As can be seen in Fig. 19 (a), even with a wide range of mismatches in the HAPF parameters (PPF capacitor and inductor and APF output inductors) the performance of the suggested controller is still acceptable and the source current THD remains within the standard range. The proposed controller adaptively changes the control gains by correcting the filter parameters. As can be seen in Figs. 19 (b), (c) and (d), when HAPF parameters change, the performance of the other

TABLE II
Comparison among different current controllers

Criterion / Current Controller	Grid current THD (%)	Current tracking error (%)	Control run time (µs)	Performance under parameters changes	Disadvantages
P [7]-[9]	7.5%	9.8%	0.15	Medium	- high current tracking error - weak at transients
PR [5], [10], [19]	6%	5.9%	1.5	Weak	- slow response - sensitive to frequency changes
Improved Deadbeat [6], [12]	5.4%	4.5%	0.85	Very weak	- very sensitive to system parameters - low stability region for the controller gain
Proposed method	3.7%	2.3%	5.6	Excellent	- relatively complex

current controllers degrades significantly and their parameters should be modified accordingly.

Table II compares the proposed current control technique with three different current controllers. The grid current THDs in this table are obtained for the single-phase nonlinear load depicted at the beginning of this section. As can be seen, the performance of the proposed controller, current tracking error and its grid current THD are all better than the other control techniques. Although, the control code execution time for the proposed method is higher than the other techniques, however this time is less than 10% of the sampling period. So, the proposed technique can be easily implemented on a medium-performance floating-point digital signal controller.

VI. Conclusion

This paper proposed an adaptive STC technique for the current tracking of an LCL-filtered LC-tuned single-phase shunt HAPF. The proposed digital technique offers ease of implementation and excellent steady-state and transient performance that is not affected by the parameters' mismatches. The system parameters are identified online and a systematic design procedure for the STC parameters is proposed accordingly. Also, improved formula for the adaptive control law is suggested, which ensures proper rejection of grid voltage disturbances. Then, the HAPF parameters design is described considering the LCL filter stability requirements and the overall closed-loop control stability in the discrete domain is discussed considering the digital control delay. The effectiveness of the suggested control technique is confirmed through simulation and experimental tests. Furthermore, a comprehensive comparison between the proposed method and three other ones is provided to show the superiority of the proposed technique in different aspects.

VII. References

[1] J. C. Das, "Passive filters—potentialities and limitations," *IEEE Trans. Ind. Appl.*, vol. 40, no. 1, pp. 232–241, Jan. 2004.

[2] H. Hu, Z. He, and S. Gao, "Passive filter design for china high-speed railway with considering harmonic resonance and characteristic harmonics," *IEEE Trans. Power Deliv.*, vol. 30, no. 1, pp. 505–514, Feb. 2015.

[3] X. Li, W. Xu, and T. Ding, "Damped high passive Filter—a new filtering scheme for multipulse rectifier systems," *IEEE Trans. Power Deliv.*, vol. 32, no. 1, pp. 117–124, Feb. 2017.

[4] M. Badoni, A. Singh, and B. Singh, "Variable forgetting factor recursive least square control algorithm for DSTATCOM," *IEEE Trans. Power Deliv.*, vol. 30, no. 5, pp. 2353–2361, Oct. 2015.

[5] M.-S. Karbasforooshan and M. Monfared, "Multi-resonant indirect digital current control technique for single-phase shunt active power filters," *Electr. Power Components Syst.*, vol. 47, no. 13, pp. 1196–1202, Nov. 2019.

[6] M.-S. Karbasforooshan and M. Monfared, "An improved reference current generation and digital deadbeat controller for single-phase shunt active power filters," *IEEE Trans. Power Deliv.*, vol. 35, no. 6, pp. 2663–2671, Dec. 2020.

[7] R. Inzunza and H. Akagi, "A 6.6-kV transformerless shunt hybrid active filter for installation on a power distribution system," *IEEE Trans. Power Electron.*, vol. 20, no. 4, pp. 893–900, Jul. 2005.

[8] W. Tangtheerajaroonwong, T. Hatada, K. Wada, and H. Akagi, "Design and performance of a transformerless shunt hybrid filter integrated into a three-phase diode rectifier," *IEEE Trans. Power Electron.*, vol. 22, no. 5, pp. 1882–1889, Sep. 2007.

[9] T.-L. Lee, Y.-C. Wang, J.-C. Li, and J. M. Guerrero, "Hybrid active filter with variable conductance for harmonic resonance suppression in industrial power systems," *IEEE Trans. Ind. Electron.*, vol. 62, no. 2, pp. 746–756, Feb. 2015.

[10] L. Herman, I. Papic, and B. Blazic, "A proportional-resonant current controller for selective harmonic compensation in a hybrid active power filter," *IEEE Trans. Power Deliv.*, vol. 29, no. 5, pp. 2055–2065, Oct. 2014.

[11] Lei Hong, Ye Tian, Jing Zhang, Dujiang Li, Dehong Xu, and Guozhu Chen, "High precision compensation for high power Hybrid Active Power Filter based on repetitive control algorithm," in *2011 IEEE International Symposium on Industrial Electronics*, pp. 295–300, 2011.

[12] W.-K. Sou, W.-H. Choi, C.-W. Chao, C.-S. Lam, C. Gong, C.-K. Wong, and M.-C. Wong, "A deadbeat current controller of LC-hybrid active power filter for power quality improvement," *IEEE J. Emerg. Sel. Top. Power Electron.*, vol. 8, no. 4, pp. 3891–3905, Dec. 2020.

[13] P. Dey and S. Mekhilef, "Shunt hybrid active power filter under nonideal voltage based on fuzzy logic controller," *Int. J. Electron.*, vol. 103, no. 9, pp. 1–13, Feb. 2016.

[14] S. C. Ferreira, R. B. Gonzatti, R. R. Pereira, C. H. da Silva, L. E. B. da Silva, and G. Lambert-Torres, "Finite control set model predictive control for dynamic reactive power compensation with hybrid active power filters," *IEEE Trans. Ind. Electron.*, vol. 65, no. 3, pp. 2608–2617, Mar. 2018.

[15] A. Hamadi, S. Rahmani, and K. Al-Haddad, "Digital control of a shunt hybrid power filter adopting a nonlinear control approach," *IEEE Trans. Ind. Informatics*, vol. 9, no. 4, pp. 2092–2104, Nov. 2013.

[16] C. Gong, W.-K. Sou, and C.-S. Lam, "Second-order sliding mode current controller for LC-coupling hybrid active power filter," *IEEE Trans. Ind. Electron.*, vol. 0, no. 0, pp. 1–11, 2020 (DOI: 10.1109/TIE.2020.2972430).

[17] J. Wu, H. Jou, K. Wu, and H. Hsiao, "Three-phase four-wire hybrid power filter using a smaller power converter," *Electr. Power Syst. Res.*, vol. 87, pp. 13–21, Jun. 2012.

[18] Y. Deng, X. Tong, and H. Jia, "A bidirectional control principle of active tuned hybrid power filter based on the active reactor using active techniques," *IEEE Trans. Ind. Informatics*, vol. 11, no. 1, pp. 141–154, Feb. 2015.

[19] A. A. Valdez-Fernandez, G. Escobar, P. R. Martinez-Rodriguez, J. M. Sosa, D. U. Campos-Delgado, and M. J. Lopez-Sanchez, "Modelling and control of a hybrid power filter to compensate harmonic distortion under unbalanced operation," *IET Power Electron.*, vol. 10, no. 7, pp. 782–791, Jun. 2017.

[20] A. Hajizadeh, A. H. Shahirinia, N. Namjoo, and D. C. Yu "Self-tuning indirect adaptive control of non-inverting buck–boost converter," *IET Power Electron.*, vol. 8, no. 11, pp. 2299–2306, Nov. 2015

[21] M. Ahmeid, M. Armstrong, S. Gadoue, and M. Al-Greer, "Computationally efficient self-tuning controller for DC–DC switch mode power converters based on partial update kalman filter," *IEEE Trans. Power Electron.*, vol. 33, no. 9, pp. 8081–8090, Sep. 2018.

[22] S. W. Zhao, N. C. Cheung, W.-C. Gan, and J. M. Yang, "High-precision position control of a linear-switched reluctance motor using a self-tuning regulator," *IEEE Trans. Power Electron.*, vol. 25, no. 11, pp. 2820–2827, Nov. 2010.

[23] A. H. M. A. Rahim, E. P. Nowicki, and O. P. Malik, "Enhancement of power system dynamic performance through an on-line self-tuning adaptive SVC controller," *Electr. Power Syst. Res.*, vol. 76, no. 9–10, pp. 801–807, Jun. 2006.
[24] D. Rai, R. Gokaraju, and S. O. Faried, "Adaptive control using constrained RLS and dynamic pole-shift technique for TCSCs," *IEEE Trans. Power Deliv.*, vol. 29, no. 1, pp. 224–234, Feb. 2014.
[25] C.-H. Liu and Y.-Y. Hsu, "Design of a self-tuning PI controller for a STATCOM using particle swarm optimization," *IEEE Trans. Ind. Electron.*, vol. 57, no. 2, pp. 702–715, Feb. 2010.
[26] U. Malhotra and R. Gokaraju, "An add-on self-tuning control system for a UPFC application," *IEEE Trans. Ind. Electron.*, vol. 61, no. 5, pp. 2378–2388, May 2014.
[27] K. J. Åström, and B. Wittenmark, *Adaptive Control*, Second Edition, Mineola, N.Y., USA: Dover Publications Inc., 2008.
[28] R. D. Dorf, and R. H. Bishop, *Modern Control Systems*, 12th Edition, Prentice-Hall, Inc., 2011.
[29] Y. Han, M. Yang, H. Li, P. Yang, L. Xu, E. A. A. Coelho, and J. M. Guerrero, "Modeling and stability analysis of LCL-type grid-connected inverters: a comprehensive overview," *IEEE Access*, vol. 7, pp. 114975–115001, 2019.
[30] S. Jayalath and M. Hanif, "Generalized LCL-filter design algorithm for grid-connected voltage-source inverter," *IEEE Trans. Ind. Electron.*, vol. 64, no. 3, pp. 1905–1915, Mar. 2017.
[31] S. Jayalath and M. Hanif, "An LCL-filter design with optimum total inductance and capacitance," *IEEE Trans. Power Electron.*, vol. 33, no. 8, pp. 6687–6698, Aug. 2018.
[32] M. Sanatkar-Chayjani, and M. Monfared "Design of LCL and LLCL filters for single-phase grid connected converters," *IET Power Electron.*, vol. 9, no. 9, pp. 1971–1978, Jul. 2016.
[33] J. Yin, S. Duan, and B. Liu, "Stability analysis of grid-connected inverter with LCL filter adopting a digital single-loop controller with inherent damping characteristic," *IEEE Trans. Ind. Informatics*, vol. 9, no. 2, pp. 1104–1112, May 2013.
[34] C. Zou, B. Liu, S. Duan, and R. Li, "Influence of delay on system stability and delay optimization of grid-connected inverters with LCL filter," *IEEE Trans. Ind. Informatics*, vol. 10, no. 3, pp. 1775–1784, Aug. 2014.
[35] M.-S. Karbasforooshan and M. Monfared, "Design and implementation of a single-phase shunt active power filter based on PQ theory for current harmonic compensation in electric distribution networks," in *IECON 2017 - 43rd Annual Conference of the IEEE Industrial Electronics Society*, pp. 6389–6394, Oct. 2017.
[36] S. Golestan, M. Monfared, and J. M. Guerrero, "Second order generalized integrator based reference current generation method for single-phase shunt active power filters under adverse grid conditions," in *4th Power Electron. Drive Syst. Technol. Conf. (PEDSTC)*, pp. 510-517, Feb. 2013.

Mohammad-Sadegh Karbasforooshan received the B.Sc. and M.Sc. degrees (both with honors) in electrical engineering from Ferdowsi University of Mashhad, Mashhad, Iran, in 2013 and 2015, respectively.

He is currently working towards the Ph.D. degree at Ferdowsi University of Mashhad, Mashhad, Iran. His research interests include control of standalone and grid-connected inverters, active and hybrid power filters, and power quality.

Mohammad Monfared (S'07, M'10, SM'15) received the B.Sc. degree in electrical engineering from Ferdowsi University of Mashhad, Iran, in 2004, and the M.Sc. and Ph.D. degrees (both with honors) in electrical engineering from Amirkabir University of Technology, Tehran, Iran, in 2006 and 2010, respectively.

He is currently an Associate Professor at Ferdowsi University of Mashhad, Mashhad, Iran, where he has received the Best Researcher Award in 2015. His research interests include power electronics, renewable energy systems, and power quality.